POLITECNICO
MILANO 1863

SCUOLA DI INGEGNERIA INDUSTRIALE
E DELL'INFORMAZIONE

Executive Summary of the Thesis

Crystallization during fused filament fabrication of a biopolymer

Laurea Magistrale in Materials Engineering and Nanotechnology - Ingegneria dei Materiali e delle Nanotecnologie

Author: Martina Frangella

Advisor: Prof. Gianmarco Enrico Griffini

Co-advisor:

Academic year: 2023-2024

1. Introduction

Over the past two decades, biodegradable polymers have received significant attention for their potential to reduce plastic waste and mitigate environmental impacts. Among these, aliphatic polyesters stand out as particularly promising, offering a combination of biodegradability and biocompatibility along with physical and chemical properties comparable to those of conventional petroleum-based polymers.

Polybutylene succinate (PBS) is a notable biodegradable semicrystalline polyester known for its flexibility and processability. It is comparable to polyethylene (PE) in workability and shares physical properties with polyethylene terephthalate (PET). PBS is synthesized from succinic acid and 1,4-butanediol, with a chemical structure composed of repeating butylene succinate units ($C_8H_{12}O_4$).[4]

As with other semicrystalline polymers, PBS's mechanical properties and degradation rates are strongly influenced by its crystal structure, degree of crystallinity and morphology, including spherulite size and lamellar arrangement. Recent studies investigating PBS's crystallization and melting behavior through differential scanning calorimetry (DSC) have revealed multiple melting points corresponding to crystals of varying stabilities, an effect attributed to a dual morphology mechanism. This phenomenon indicates the presence of two distinct crystalline structures within the crystallized polymer, which play a critical role in its overall performance. [6]

Moreover, as a thermoplastic polymer, PBS can be processed via fused filament fabrication (FFF), an additive manufacturing technique that offers numerous advantages over conventional methods. The application of PBS in FFF represents a novel approach with significant potential to expand the use of bioplastics as alternatives to synthetic plastics, fostering sustainable solutions across various industries. However, effectively applying PBS in FFF requires a deeper understanding of its behavior throughout the processing cycle, as this directly affects the final product's mechanical properties, biodegradability and performance.[1]

This study aims to investigate the crystallization kinetics, spherulitic morphology, and growth rate of neat PBS over a wide temperature range using DSC, polarized optical microscopy (POM), and scanning electron microscopy (SEM). Additionally, FFF-printed samples are analyzed to evaluate how differ-

ent processing parameters impact the crystalline structure of the final product. By correlating the crystallization behavior observed in neat PBS with that in FFF-printed samples, this work seeks to optimize process parameters and enhance PBS's viability in additive manufacturing. Ultimately, the research contributes to a more sustainable future by facilitating the use of biodegradable polymers like PBS in advanced manufacturing and expanding the scope of sustainable solutions in industries currently dominated by synthetic plastics.

2. Materials and methods

This research was conducted at the PIMM Laboratory (Procédés et Ingénierie en Mécanique et Matériaux) of the École Nationale Supérieure d'Arts et Métiers in Paris.
Polybutylene succinate supplied by Naturplast (France) was used in the form of pellets, designated as PBE003, with a number-average molecular weight (M_n) of 19,800 g/mol and density of 1.26 g/cm^3.

2.1. Polarized Optical Microscopy (POM)

The spherulitic morphology and growth rate of PBS were studied using a Nikon LV-N100 polarized optical microscope (POM) equipped with polarized light, a first-order retardation plate, and a Linkam THMS 600 temperature controller. PBS samples were melted at 150°C for 3 minutes to erase thermal history and then quenched to the crystallization temperature (T_c) at a cooling rate of 100°C/min using nitrogen gas. Samples were held at T_c for an adequate duration to allow isothermal crystallization, controlled by LINK software.

2.2. Differential Scanning Calorimetry (DSC)

Isothermal crystallization kinetics were analyzed using a Perkin Elmer DSC 8500 differential scanning calorimeter. The instrument was calibrated with high-purity indium and zinc standards. Small samples, weighing 4.7 mg, were placed in aluminum crucibles and sealed with aluminum lids. Each sample was melted at 150°C for 5 minutes to remove thermal history, then cooled to the crystallization temperature at 150°C/min and maintained at T_c until crystallization was complete. All operations were performed under a nitrogen purge to facilitate rapid cooling.

2.3. Scanning Electron Microscopy (SEM)

Spherulitic assemblies were analyzed using a Hitachi 4800 II scanning electron microscope (SEM). To compare the two primary morphologies of PBS spherulites, blends of PBS and polyethylene oxide (PEO) were prepared to enhance the visibility of lamellae. Two formulations were studied: PBS/PEO 30/70 and PBS/PEO 70/30.
The blends were prepared via solution blending, using chloroform as the solvent to create a 2 wt% polymer solution. The solutions were cast onto glass slides and dried at room temperature for three days to ensure complete solvent evaporation. The resulting films were heated to 190°C for 2 minutes to erase any prior thermal history, then rapidly cooled to a specific T_c for isothermal crystallization. PEO was removed from the crystallized samples by etching with deionized water in two 30-minute cycles, followed by drying at room temperature. Before SEM analysis, samples were gold-coated using vacuum sputtering for 6 minutes at 1200 V and 10 mA.

2.4. Fused Filament Fabrication (FFF)

The morphology of FFF-printed samples was also examined to identify structural similarities with earlier findings. The Intamsys FUNMAT HT 3D printer was used for this study. Samples were printed at various nozzle and substrate temperatures, while maintaining a constant printing speed of 2000 mm/min and a 100% infill density. Thin films were then sliced from the printed samples using an LKB Bromma Ultrotome Nova microtome equipped with a diamond blade. The films were subsequently analyzed via POM.

3. Results and discussion

3.1. Spherulitic growth rate and morphology by POM

The spherulitic growth rate and morphology of PBS were investigated over a wide range of crystallization temperatures, from 75°C to 105°C.

The growth rate (G) of a selected crystal corresponds to the slope of the linear relationship between its diameter and time. Measurements were taken at various temperatures on the same crystal. Figure 1 shows the temperature dependence of the spherulitic growth rates, demonstrating that the growth rate decreases as the crystallization temperature increases.

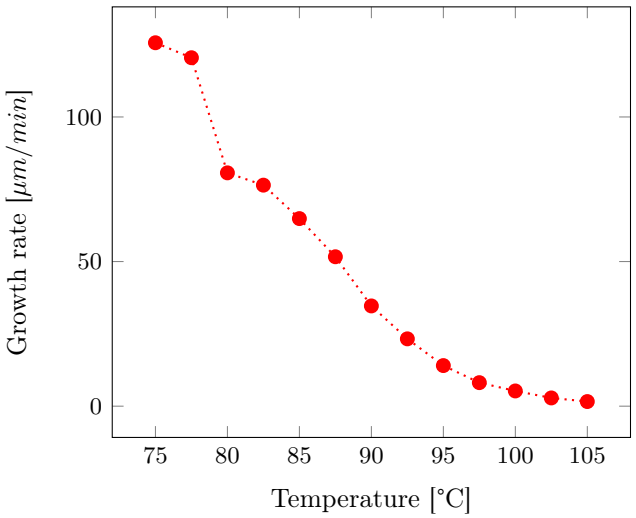

Figure 1: Growth rate vs crystallization temperature.

To further investigate the crystal growth kinetics of PBS isothermally crystallized from the melt, the spherulite growth rate can be analyzed using the secondary nucleation theory, known as the Lauritzen-Hoffman equation. According to the Lauritzen-Hoffman model, the linear growth rate (G) of a chain-folded polymer crystal is expressed as a function of the crystallization temperature (T_c) by the following equation: [2]

$$G = G_0 \exp\left[-\frac{U^*}{R(T_c - T_\infty)}\right] \exp\left[-\frac{K_g}{T_c(\Delta T)f}\right] \tag{1}$$

where G_0 represents a pre-exponential factor. The first exponential term accounts for the contribution of the diffusion process, where U^* is the activation energy required for transporting the polymer chain through the melt-crystal interface, T_∞ is a temperature below which diffusion ceases and R is the gas constant. The second exponential term reflects the contribution of the nucleation process, with ΔT representing the degree of supercooling, defined as $T_m^0 - T_c$ where T_m^0 is the equilibrium melting point and f is a correction factor accounting for the variation in the enthalpy of fusion with temperature, expressed as $f = 2T_c/(T_m^0 + T_c)$.
The parameter K_g denotes the activation energy for nucleation for a crystal of critical size and is a constant given by:

$$K_g = \frac{nb_0\sigma\sigma_e T_m^0}{\Delta h_f k} \tag{2}$$

where b_0 represents the molecular thickness, σ and σ_e are the lateral and the fold-surface free energy, respectively, and Δh_f is the bulk melting enthalpy per unit volume for a fully crystalline polymer. Here k is the Boltzmann constant and n is a constant that reflects the crystallization regime, with possible values of n=4 for regimes I and III, and n=2 for regime II. Equation 1 is typically rewritten in logarithmic form as follows:

$$lnG + \frac{U^*}{R(T_c - T_\infty)} = lnG_0 - \frac{K_g}{T_c(\Delta T)f} \tag{3}$$

Generally, two sets of values can be used for U^* and T_∞. In this work the data derived from the Williams-Landel-Ferry (WLF) equation were used, with values of $U^* = 4200$ cal/mol and $T_\infty = T_g - 51.6$ K. [5]

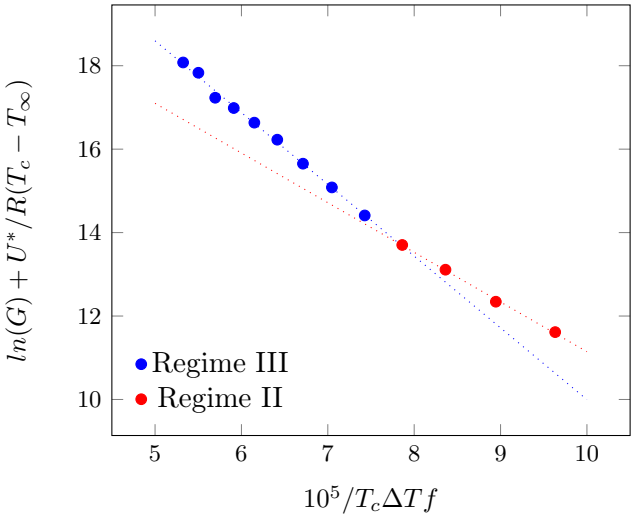

Figure 2: Lauritzen-Hoffman plot for the estimation of nucleation parameter obtained from POM measurement.

The experimental data can be well-fitted by two straight lines. The critical breakpoint indicates a regime transition accompanied by morphological changes in the formed crystal. In the

region of large supercooling, regime III is observed, while regime II is detected at smaller supercooling levels. The intersection point of the two lines represents the transition temperature $T_{III \to II}$ between the two regimes and the slopes correspond to the nucleation constant K_g for each regime. From the plot in Figure 2, the transition temperature $T_{III \to II}$ was of approximately 97°C while the ratio K_g^{III}/K_g^{II} was about 1.45.
The spherulitic morphology of PBS crystallized at 75, 80 and 90°C is shown in Figure 3.

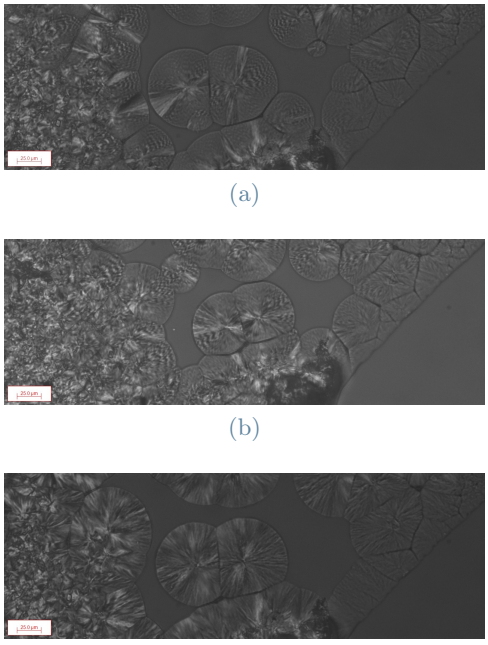

(a) (b) (c)

Figure 3: Optical micrographs of the spherulitic morphology of PBS isothermally crystallized at (a) 75, (b) 80, (c) 90°C. Same scale for all the pictures ($25\mu m$).

The size of the spherulites increases with crystallization temperature, which can be attributed to the difficulties in nucleation and the subsequent reduction in the number of nuclei. At lower crystallization temperatures (75°C), banded spherulites display concentric extinction bands, with the band spacing decreasing as the crystallization temperature decreases. At higher crystallization temperatures (90°C), the ringed bands disappear, revealing an axialite-like or dendritic structure. At intermediate temperatures (80°C), PBS exhibits a mixed structure, featuring both ring-banded and dendritic patterns. The regime transition identified through the secondary nucleation theory of Lauritzen-Hoffman can be correlated with changes in crystal morphology.

3.2. Isothermal crystallization kinetics by DSC

The overall isothermal crystallization kinetics of PBS were investigated by DSC for T_c in the range of 75-92.5°C. The exothermic curves were recorded as a function of crystallization time, t_c, for all crystallization temperatures. From that, the crystallization enthalpy (ΔH_c) was determined as a function of T_c (Figure 4). Figure 4 shows that ΔH_c increases from 72.32 J/g at 75°C to 79.05 J/g at 92.5°C. Thus, at higher temperatures more energy is required for PBS molecules to establish a stable crystalline structure.

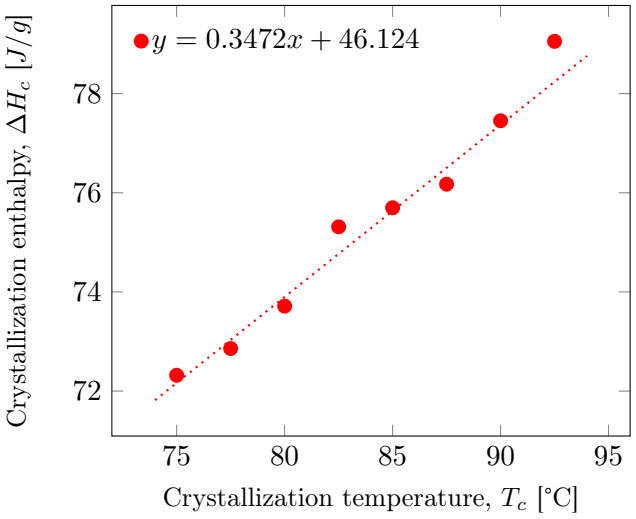

Figure 4: Crystallization temperature dependence of crystallization enthalpy.

From ΔH_c can be derived also the degree of crystallinity which mirrors the behavior of crystallization enthalpy. The degree of crystallinity of PBS increases from 36.2% to 39.5% as the crystallization temperature rises from 75°C to 92.5°C.
The Avrami model was employed to analyze the overall isothermal crystallization kinetics. The model posits that the relative degree of crystallinity, $X(t)$, evolves as a function of crystallization time according to the following equation:

$$X(t) = 1 - exp(-kt^n) \quad (4)$$

where k is the crystallization rate constant de-

pendent on both nucleation and growth rates and n is the Avrami exponent, which reflects the mechanisms of nucleation and the morphology of crystal growth.
Figure 5 illustrates the development of $X(t)$ as a function of crystallization time. It is evident that t_c increases with rising T_c, indicating that the crystallization process is retarded at higher temperatures.

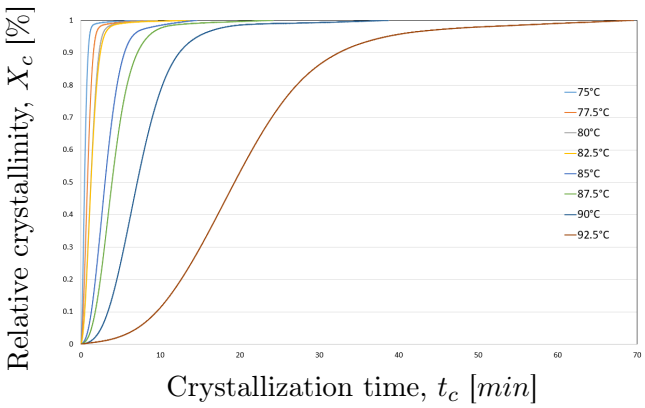

Figure 5: Development of relative degree of crystallinity (X_c) as a function of crystallization time (t_c).

The Avrami equation can be written also as:

$$\ln\left(-\ln\left(1-X(t)\right)\right) = n\ln\left(t\right) + \ln\left(k\right) \qquad (5)$$

where the Avrami parameters n and k can be determined from the slope and intercept, respectively, as shown in Figure 6.
PBS kinetic data are summarised in Table 1.
The values of n range between 1.6 and 2.6. This variation indicates that spherulites exhibit three-dimensional growth only at temperatures exceeding approximately 85°C, where the n value exceeds 2. This observation is corroborated by the POM analyses, which reveal that the morphology of the spherulites transitions from ring-banded to dendritic structures as the temperature increases. Moreover, the values of k decrease with rising crystallization temperature, suggesting that crystallization is delayed at higher temperatures.

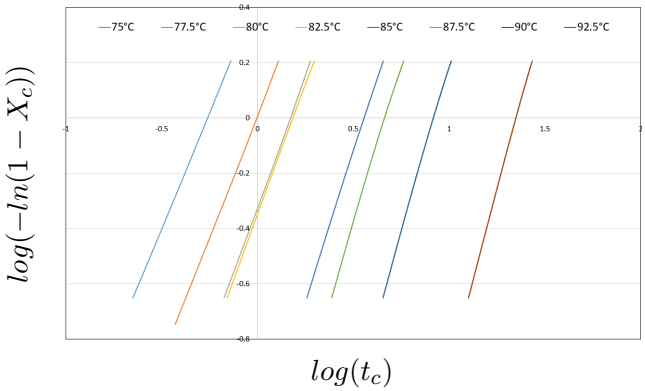

Figure 6: Avrami plot.

T_c [°C]	n	k [min^{-n}]	t_{max} [min]	$t_{1/2}$ [min]	$(t_{1/2})^{-1}$ [min^{-1}]
75	1.68	2.749	0.320	0.441	2.269
77.5	1.77	1.0184	0.617	0.804	1.243
80	1.90	0.474	0.999	1.222	0.818
82.5	1.89	0.449	1.024	1.259	0.794
85	2.14	0.064	2.688	3.036	0.329
87.5	2.28	0.031	3.588	3.934	0.254
90	2.41	0.006	6.643	7.127	0.140
92.5	2.59	0.0003	18.515	19.404	0.051

Table 1: Parameters n, k, t_{max} and $t_{1/2}$, from the Avrami analysis of isothermal melt crystallization.

Additionally, the maximum crystallization time, t_{max}, can be calculated using the n and k parameters according to the following equation:

$$t_{max} = \left(\frac{n-1}{nk}\right)^{1/n} \qquad (6)$$

It can be observed that the values of t_{max} increase with the crystallization temperature. The half-life crystallization time, $t_{1/2}$, defined as the time elapsed from the onset of crystallization to the point where crystallization is half-completed can also be calculated using the relation:

$$t_{1/2} = \left(\frac{ln2}{k}\right)^{1/n} \qquad (7)$$

To compare crystallization rates, we used the reciprocal half-time of crystallization, $1/t_{1/2}$. The values of $1/t_{1/2}$ are plotted in Figure 7 as functions of crystallization temperature. The value of $1/t_{1/2}$ decreases with increasing crystallization temperature, reflecting a reduction in the crystallization rate.

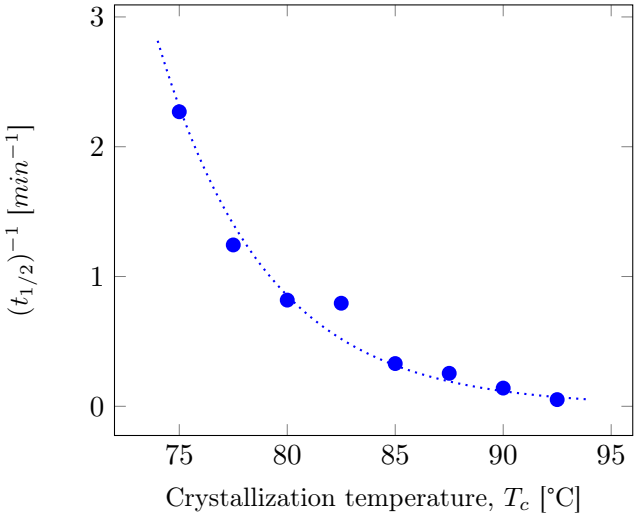

Figure 7: Crystallization temperature dependence of $(t_{1/2})^{-1}$.

3.3. Spherulites assembly by SEM

The lamellar assembly was examined on PBS/PEO blend with composition of 30/70 and 70/30 using SEM. The 30/70 blend was selected to visualize the dendritic pattern, while the 70/30 blend was chosen to examine the ring-banded pattern. Both blends were crystallized isothermally at 75°C.

The dendritic pattern consists of two types of crystal branches, described as feather-like and fern-like. [3] The feather-like lamellar stacks exhibit a fully edge-on orientation, whereas the fern-like branches are composed of flat-on crystals. Figure 8 shows the top surface of two spherulites from the PBS/PEO 30/70 blend, clearly distinguishing the two types of branches: edge-on and flat-on. Both the configuration can coexist on the same branch. Regarding the feather-like pattern, as the spherulitic radius increases, the number of small edge-on branches also increases to fill the available space. In the case of the fern-like pattern, as the spherulitic radius grows, the length of the side branches expands to cover the larger area.

The 70/30 PBS/PEO blend exhibits the ring-banded structure but the visualization of single spherulite was more challenging due to the lower amount of PEO. However, the ring-banded pattern is identifiable by the band spacing, which is characterized by ridge regions, where the lamellae are likely oriented vertically (edge-on), and valley regions, where they are likely oriented horizontally (flat-on).

Comparing the two main morphologies, the ring-banded structure grows along the sheaf-nuclei direction, while dendritic structures grow perpendicular to the sheaf-nuclei direction.

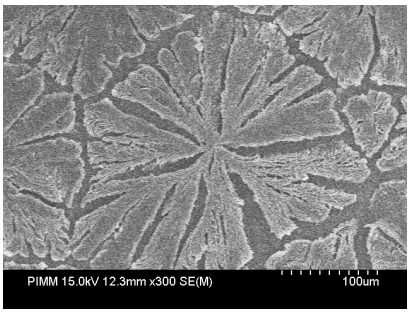

(a)

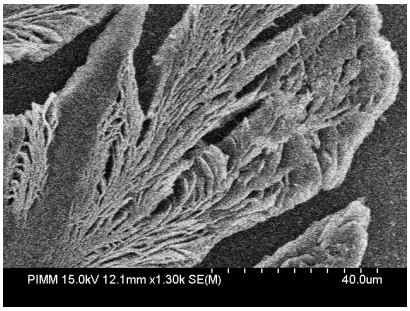

(b)

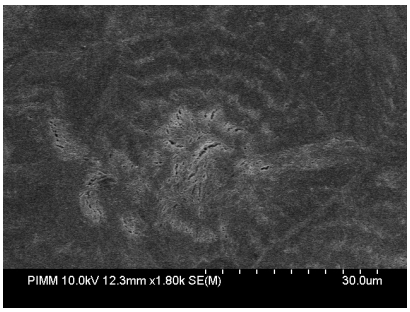

(c)

Figure 8: SEM graphs of the top surface of spherulite crystallized at T_c=75°C of:
(a) 30/70 PBS/PEO blend (scale of 100 μm),
(b) 30/70 PBS/PEO blend (scale of 40 μm), and
(c) 70/30 PBS/PEO blend (scale of 30 μm).

3.4. Spherulitic morphology of FFF printed samples

PBS samples printed via Fused Filament Fabrication were analyzed using POM to compare the results with previous findings, aiming to understand the influence of different process parameters on the spherulitic morphology and to optimize these parameters. In this study, the nozzle and substrate temperatures were varied to eval-

uate their effects on the morphological structure of the samples. Six samples were printed while maintaining a constant substrate temperature (T_s) to simulate isothermal crystallization conditions.
For the first three samples, the nozzle temperature (T_n) was fixed at 230°C, while T_s was varied between 75°C, 90°C and 110°C to investigate its influence on spherulitic morphologies. Observations of the resulting films using POM revealed that the spherulitic microstructure was difficult to discern, likely due to the overlapping of multiple printed layers, which obscures individual spherulites (Figure 9a, 9b, 9c). However, changes in the birefringence index were evident when T_s was varied, suggesting differences in the degree and orientation of crystallinity. Higher T_s values resulted in slower crystallization rates, potentially leading to a more stable crystalline structure.
For the remaining three samples, the substrate temperature was kept constant at 110°C, while T_n was varied between 175°C, 190°C and 230°C. The POM images obtained from this study did not provide sufficient evidence to establish a direct correlation between T_n and the spherulitic microstructural characteristics (Figure 9c, 9d, 9e).

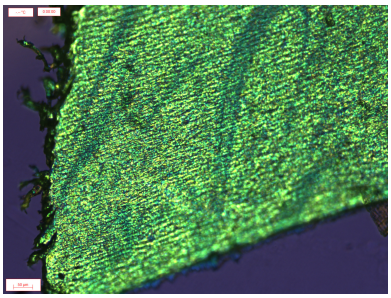

(a)

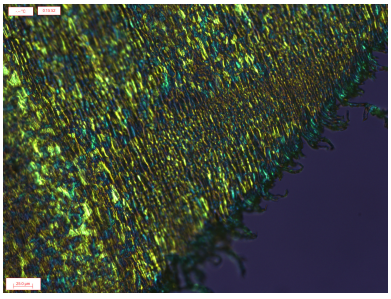

(b)

Across all samples, a striated microstructure was observed, likely attributable to the layer-by-layer printing technique. However, individual spherulites were not evident, making it challenging to directly correlate the observed morphology with specific process parameters.

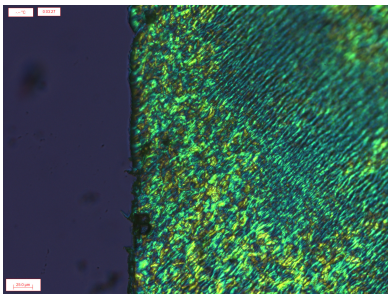

(c)

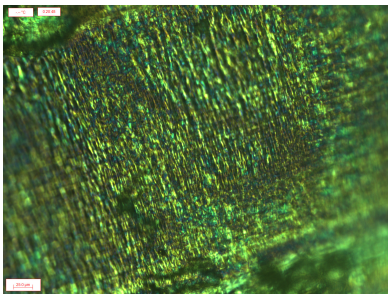

(d)

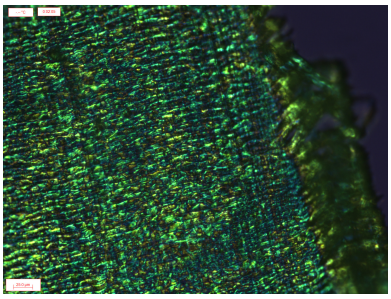

(e)

Figure 9: POM micrographs with magnification of 25 μm of 3D printed sample at:
(a) T_s=75°C and T_n=230°C;
(b) T_s=90°C and T_n=230°C;
(c) T_s=110°C and T_n=230°C;
(d) T_s=110°C and T_n=175°C;
(e) T_s=110°C and T_n=190°C.

4. Conclusion and future work

The isothermal crystallization kinetics and spherulitic morphology of PBS were investigated using DSC, POM and SEM.
The growth rate of spherulites was observed using POM for T_c values ranging from 75°C to 105°C. It was found that an increase in crystallization temperature corresponded to a decrease in the spherulitic growth rate. Further-

more, applying the secondary nucleation theory revealed the presence of two distinct crystallization regimes, regime II and regime III, with a transition temperature near 97°C. This transition was also reflected in the spherulitic morphology, which exhibited two main configurations: at lower temperatures, a ring-banded structure with a higher number of nuclei was predominant, while at higher temperatures, a dendritic structure with fewer and coarser nuclei became dominant.

Crystallization kinetics were studied using DSC and analyzed through the Avrami equation over a temperature range of 75°C to 92.5°C. The Avrami exponent (n) was found to range between 1.6 and 2.6. Values exceeding 2, observed at temperatures above approximately 85°C, indicated three-dimensional spherulitic growth, resulting in a dendritic structure. A transition from three-dimensional to two-dimensional growth was identified around 85°C, corresponding to the shift from ring-banded to axialite-like morphology.

SEM analysis of PBS/PEO blends revealed both ring-banded and dendritic morphologies. The dendritic structure consisted of two types of crystal branches: feather-like (fully edge-on) and fern-like (flat-on). In contrast, the ring-banded was characterized by ridge (edge-on lamellae) and valley (flat-on lamellae) regions.

Finally, PBS samples were printed using the Fused Filament Fabrication (FFF) technique. The nozzle and substrate temperatures were varied to assess their influence on the structural characteristics, while other parameters were held constant. Films revealed that variations in nozzle and substrate temperatures did not significantly alter the overall structure of PBS. However, differences in the birefringence index among samples printed at different T_s suggested variations in the degree and orientation of crystallinity. Despite these observations, spherulitic morphology under differing process parameters remained indistinct.

Future research should aim to identify specific process parameters that can effectively control the morphological structure of PBS in FFF-printed objects, enabling the production of materials with tailored crystal structures. Additionally, extending this investigation to a broader range of biodegradable polymers and polymer blends could enhance the sustainability and functionality of materials employed in additive manufacturing.

References

[1] Daniela Fico, Daniela Rizzo, Raffaele Casciaro, and Carola Esposito Corcione. A review of polymer-based materials for fused filament fabrication (fff): Focus on sustainability and recycled materials. *Polymers*, 14, 2022.

[2] John D. Hoffman and Robert L. Miller. Kinetic of crystallization from the melt and chain folding in polyethylene fractions revisited: theory and experiment. *Polymer*, 38(13):3151–3212, 1997.

[3] Hsiao-Hua Li, Selvaraj Nagarajan, Wei-Tsung Chuang, Yi-Wei Tsai, and Eamor M Woo. Microscopic and small-/wide-angle microbeam x-ray analyses on dendritic crystals in poly (butylene succinate). *Macromolecules*, 56(4):1471–1480, 2023.

[4] S. Ayu Rafiqah, Abdan Khalina, Ahmad Saffian Harmaen, Intan Amin Tawakkal, Khairul Zaman, M. Asim, M.N. Nurrazi, and Ching Hao Lee. A review on properties and application of bio-based poly(butylene succinate). *Polymers*, 13(9), 2021.

[5] ML Williams, RF Landel, and JD Ferry. Mechanical properties of substances of high molecular weight. 19. the temperature dependence of relaxation mechanisms in amorphous polymers and other glass-forming liquids. *Journal of the American Chemical Society*, 77(14):3701–3707, 1955.

[6] Gan Zhihua, Abe Hideki, Kurokawa Haruhiko, and Doi Yoshiharu. Solid-state microstructures, thermal properties, and crystallization of biodegradable poly(butylene succinate) (pbs) and its copolyesters. *Biomacromolecules*, 2:605–613, 2001.